ACS APPLIED MATERIALS & INTERFACES

RESEARCH ARTICLE

www.acsami.org

Melt Blending In situ Enhances the Interaction between Polystyrene and Graphene through $\pi-\pi$ Stacking

Bin Shen, Wentao Zhai,* Cao Chen, Dingding Lu, Jing Wang, and Wenge Zheng*

Ningbo Key Lab of Polymer Materials, Ningbo Institute of Material Technology and Engineering, Chinese Academy of Sciences, Ningbo, Zhejiang province, 315201, China

Supporting Information

ABSTRACT: The effect of melt blending on the interaction between graphene and polystyrene (PS) matrix has been investigated in this paper. The interaction between graphene and PS was significantly enhanced by melt blending, which led to an increased amount of PS-functional graphene (PSFG) exhibiting good solubility in some solvents. The PS chains on PSFG could effectively prevent the graphene sheets from aggregating and the prepared PS/PSFG composites exhibited a homogeneous dispersion and an improved electrical property. The mechanism of melt blending on this enhanced interaction was attributed to the formation of $\pi-\pi$ stacking during the melt blending. Moreover, the formation of chemical bonding during melt blending may have also enhanced the interaction.

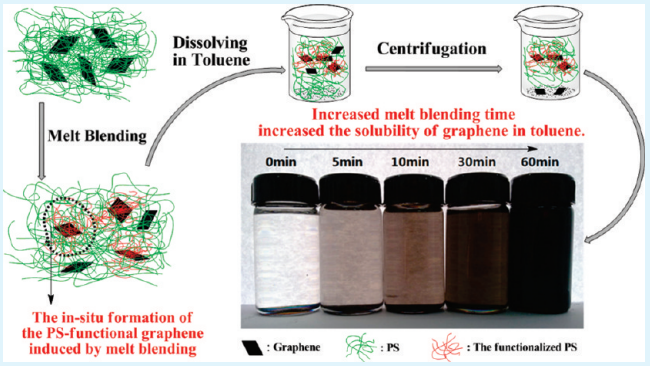

KEYWORDS: graphene, polystyrene, melt blending, interactions, $\pi-\pi$ stacking

1. INTRODUCTION

Graphene, characterized by an atomically thin two-dimensional sheet of sp^2 atoms, is regarded as "the thinnest material in the universe" with tremendous potential applications.[1,2] Because of its high surface area and high aspect ratio, excellent tensile strength, well-defined thermal conductivity, and electrical conductivity, graphene is considered useful in various technological areas, such as electonics, sensors, solar cells, memory devices, hydrogen storage, and polymer composites.[3−7] All these wonderful characteristics make graphene very promising in the scientific community.

To achieve those unique properties, however, the key issue is to well-disperse the graphene and utilize it as a nanoreinforcement. Unfortunately, graphene as a bulk material has a pronounced tendency to agglomerate because of its high surface energy, and the proper dispersion of graphene in polymer matrix is still challenging.[8−10] Three approaches have been attempted to achieve this, such as in situ polymerization,[11] melt blending[12] and solution mixing.[13,14] Among them, melt blending is the most attractive choice because it presents high efficiency, easy scale up, and no solvent is required during the processing.

High-temperature and strong shear forces are usually involved during the melt blending process, which tends to fracture the nanoparticle aggregates, and endow polymer chains with the ability to diffuse into the gaps of the nanoparticle interlayer. Furthermore, as suggested by theoretical and experimental studies,[15,16] chemical or physical interactions can be formed between the fillers and the polymer components. In the study of polycarbonate (PC)/carbon nanotube (CNT) composites, Ding et al.[17] investigated the in situ induction formation of interactions between PC and CNT by melt compounding. Based on the scanning electron microscope (SEM) observation, they observed an annular coating on the CNT, which was considered a direct proof of polymer sheathing in CNT. In another study of polystyrene (PS)/CNT carried out by Zhang et al.,[18] the researchers found that the melt blending dramatically increased the solubility of CNT in solvents. Graphene sheets have much larger size and surface areas than that of CNT, which may prevent the dispersion of the graphene in the polymer matrix, as no specific interactions can be formed between them. Thus, inducing an interaction between the graphene and polymers by way of melt blending in situ would be critical to broadening the graphene's applications. To the best of our knowledge, however, there are no such results reported so far, despite an explosive increase in the study of polymer/graphene composites.[19−25]

In this study, PS, one of the most commonly used commercial polymers, was selected as the polymer matrix and the PS/graphene composites (PSG) were prepared via solution mixing and melt blending. The resultant samples were systematically assessed by various characterization techniques and the influence of melt blending on the interaction between PS and graphene was investigated. The formation mechanism of the interaction between PS and graphene will be discussed.

Received: May 16, 2011
Accepted: July 11, 2011
Published: July 11, 2011

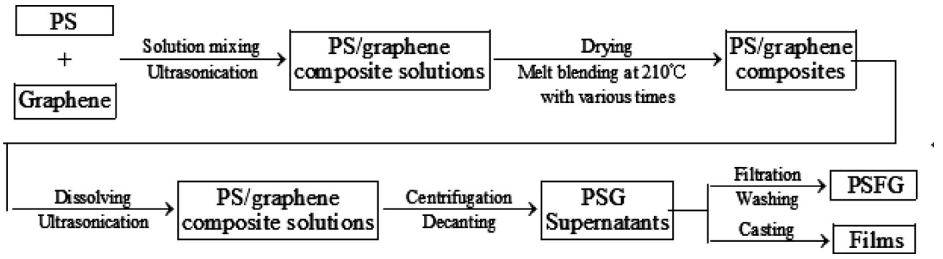

Figure 1. Experimental procedure for the preparation of samples.

2. EXPERIMENTAL SECTION

2.1. Materials. Graphene sheets were prepared according to the method described in our previous work[26] (see the Supporting Information). The C/O ratio of the graphene was 13.2, measured with a Shimadzu Axia-Ultra DLD X-ray photoelectron spectroscopy. And the specific surface area is ~700 m^2/g measured with a Micromeritics ASAP 2010 analyzer (Norcross, GA) by the Brunauer−Emmett−Teller (BET) method using nitrogen adsorption. This is about ~3.5 times lower than the ideal specific surface area (2630 m^2/g) of a single graphene sheet,[27] which indicates that each graphene platelet is comprised of ~3−4 individual graphene sheets on average. General grade PS pellets, having a number-average molecular weight (M_n) of 179 600 with a polydispersity index (M_w/M_n) of 1.79, was purchased from Shanghai SECCO Petrochemical Company Limited (China) and dried at 80 °C under vacuum for 24 h before use. Fuming nitric acid (63%), sulfuric acid (98%), potassium chlorate (98%), hydrochloric acid (37%), toluene, chloroform ($CHCl_3$), tetrahydrofuran (THF), and ethanol were obtained from Sinoparm Chemical Reagent (China).

2.2. Preparation of the PSG Samples. The experimental procedure of the preparation of the samples is illustrated in Figure 1. Graphene is a material with a low bulk density, and feeding large amounts of graphene into the polymer melt is difficult, especially in the case of high loading. Therefore, the PSG composites were first prepared by a solution blending with a graphene loading of 5 wt %, and THF was used as a solvent because of its high graphene solubility and low toxicity. First, graphene (1.0 g) was mixed in THF (200 mL) at room temperature with the aid of ultrasonication (200 W, 40 kHz) for 24 h. Then, PS (19.0 g) was dissolved into graphene suspension by vigorous stirring. After that, the resultant solution was precipitated in excessive ethanol and the precipitate was dried at 80 °C under a vacuum for 48 h. Finally, the composites with 5 wt % graphene were melt blended at 210 °C using a mini-lab scale twin-screw extruder (SJZS-10, Wuhan Rayzone Ming Plastics Machinery Co., Ltd., China) for various times, i.e., 0, 5, 10, 30, and 60 min, and the prepared samples were coded as PSG0, PSG5, PSG10, PSG30, and PSG60, respectively. The same amount of PSG composites with various melt blending times were dissolved in toluene. Ultrasonication (200 W, 40 kHz, 0.5 h) of these composite solutions in a water bath produced dark suspensions. Some of these dark PSG suspensions were filtrated with a 220 nm polytetrafluoroethylene (PTFE) membrane to collect the PS filtrate and the PS filtrate was precipitated in excessive ethanol and dried at 80 °C under vacuum for GPC measurement. Other dark suspensions were centrifuged at 8000 rpm for 30 min, and the supernatants were decanted. A small amount of the supernatant solutions were slowly dropped onto the cleaned glass plates, and kept at 80 °C under vacuum for 48 h to remove any remnant toluene. The prepared films were peeled off the substrate for the thermogravimetric analysis (TGA) measurement. Other supernatant solutions were also filtrated with a 220 nm PTFE membrane. Then, the obtained PS-functional graphene (PSFG) was washed with toluene more than 10 times to remove any free PS. After that, the PSFG was dried at 80 °C for 24 h under a vacuum. According to the various melt blending times, the obtained PSFG samples were coded as PSFG5, PSFG10, PSFG30, and PSFG60, respectively.

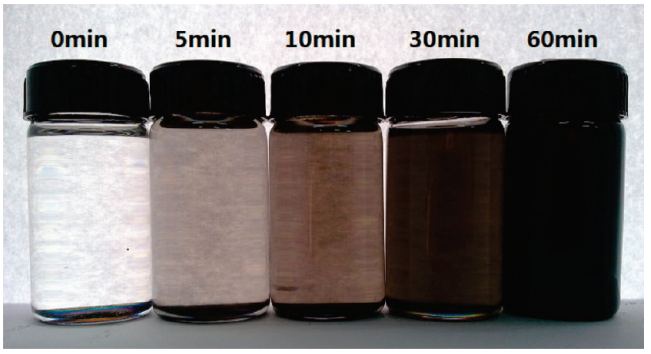

Figure 2. Digital photos of the PSG/toluene supernatants obtained by centrifugated at 8000 rpm for 30 min.

2.3. Characterizations. The TGA measurements were conducted at 20 °C/min from room temperature to 600 °C under a nitrogen flow (40 mL/min) using a Mettler-Toledo TG/DSC 1 thermogravimetric analyzer (Switzerland). FT-IR spectra (KBr) were collected with a Thermo Nicolet Nexus 6700 instrument. TEM images were taken with a Tecnai G2 F20 transmission electron microscope with an accelerating voltage of 100 kV. Graphene sheets were dispersed in $CHCl_3$ by sonication and some pieces were collected on carbon-coated 300-mesh copper grids for observation. Although for PS/graphene composites, the samples were embedded in epoxy resin, and cured at 80 °C for 6 h, and then ultrathin sections thinner than 100 nm were cryogenically cut with a diamond knife using a microtome and collected on 300-mesh copper grids. Optical observation of the thin films was performed on an Olympus BX 51TF microscope equipped with a camera DP71. The conductivity of PS composites with a dimension of 10 mm × 12 mm × 1 mm was measured using a standard four-probe method on a Physical Property Measurement System (Quantum Design, US). The ultraviolet−visible (UV−vis) spectra were recorded on a computer-controlled spectrophotometer (Perkin-Elmer Lambda 950), using $CHCl_3$ as a reference solution. The scanned area was from 200 to 800 nm. GPC experiments were determined by Gel permeation chromatography (GPC, Waters Breeze 1515). THF was used as an eluent and the PS standard for calibration.

3. RESULTS

In the present study, in order to show the effect of melt blending on the interaction of graphene and PS, the PSG composites were first prepared by solution mixing, followed by a melt blending with different times (t = 0, 5, 10, 30, 60 min). Under ultrasonication for 30 min, black suspensions were obtained. After centrifugation, the supernatants were decanted. The optical photos of these supernatants are shown in Figure 2.

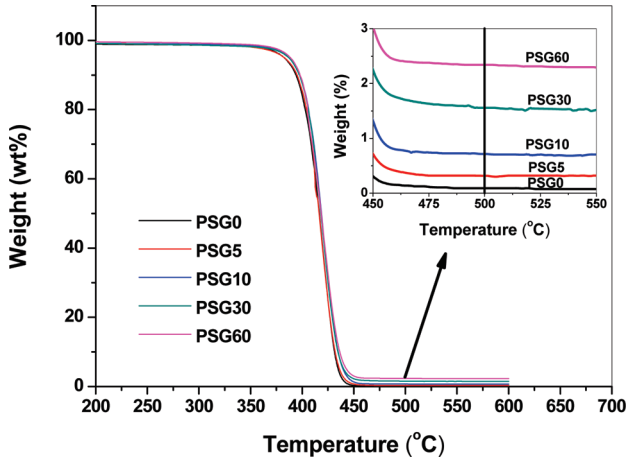

Figure 3. TGA curves of films casted from the PSG/toluene supernatants obtained by centrifugation at 8000 rpm for 30 min. The PSG composites were prepared by melt blending for 0, 5, 10, 30, and 60 min, respectively.

Table 1. Dissolved Graphene and the Functionalized PS in PSFG Samples with Various Melt Blending Times

melt blending time (min)	dissolved graphene content in PSG sample (wt %)	functionalized PS content in PSFG sample (wt %)
5	0.24	7.1
10	0.65	10.1
30	1.53	18.0
60	2.34	44.5

The supernatant solution obtained by centrifugating the PSG0 sample without melt blending is colorless and transparent, indicating the absence of graphene in the supernatant. However, melt blending of only 5 min (PSG5) yielded a slight black but transparent supernatant solution, implying that some graphene became soluble in toluene. Prolonging the time of melt blending (from 5 to 60 min) resulted in a dramatic enhancement of the solubility of graphene in toluene, characterized by visually homogeneous and transparent solutions of PS/graphene complex in black ranging from light to dark. These dark-colored supernatant solutions remained stable and homogeneous even for three months and longer.

The graphene content in the supernatant solutions of PSG samples were calculated quantitatively by TGA. Prior to the study, the supernatants were casted into films. As shown in Figure 3, the TGA curves decrease rapidly at 350−450 °C and then level off at temperature higher than 500 °C. This suggested that the bulk PS had been decomposed completely and the residues at 500−600 °C were considered to be graphene as well as the formed carbon, since the experiments were carried out at the nitrogen atmosphere. The inserted figure shows the partial enlarged view, and the graphene content was obtained by taking out the carbon content. Table 1 shows the graphene content in the casted PSG films. It is seen that the dissolved graphene content is 0.24 wt % for PSG5, and the extended melt blending time gradually increases the value to 0.65 wt % for PSG10, and to 1.53 wt % for PSG30, and to 2.34 wt % for PSG60, respectively. These results further verified that the extension of melt blending

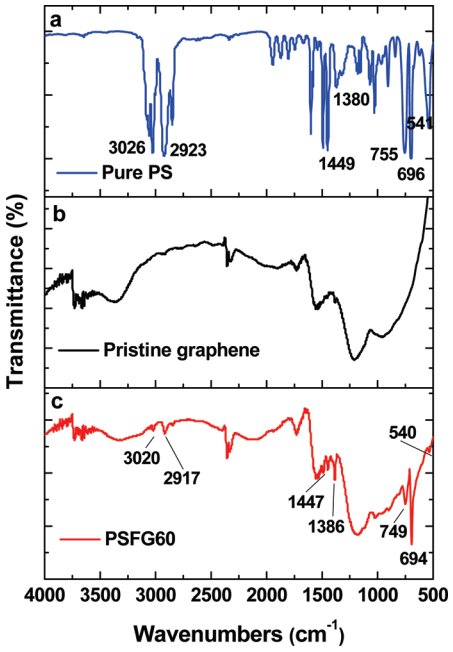

Figure 4. FT-IR spectra of (a) pure PS, (b) pristine graphene, and (c) PSFG60.

time enhanced the solubility of graphene in the supernatant solutions.

The pristine graphene could not dissolve in toluene, whereas the melt blending of graphene with PS facilitated the dissolution process of graphene in toluene. This suggests that melt blending strengthened the interaction between PS and graphene, and resulted in the formation of PS-functional graphene (PSFG), which led to an improved solubility of graphene in toluene. Moreover, the stabilization against van der Waals attraction, which is essentially provided by steric hindrance of the functionalized PS chains (the functionalized PS is the PS chains coating on the surface of PSFG through the interaction between PS and graphene by melt blending), can prevent the agglomeration of PSFG in the supernatant solutions. That is why the supernatant solutions remained stable and homogeneous for months. It should also be noted that, in practice, the melt blending of graphene and PS also yields part of graphene in other solvents, such as $CHCl_3$ and THF, indicating the melt blending is the main reason that led to enhanced interactions between graphene and PS components. In the following segments, the PSFG were characterized by FT-IR spectra and TEM observation, and the functionalized PS coating on the PSFG were quantified.

Figure 4 illustrates the FT-IR spectra of pristine graphene and PSFG60 samples. Before the FT-IR measurements of PSFG60 powder sample were taken, the PSFG60 was washed with toluene until no PS remnant in the filtrate could be detected by UV−vis spectra. Compared to the pristine graphene (Figure 4b), prominent multiple characteristic peaks are observed in PSFG60 sample (Figure 4c). The four peaks at 694, 749, 1386, and 1447 cm^{-1} correspond to the absorption of the benzene ring of the PS segments (Figure 4a). In addition, the peaks at 2917 and 3020 cm^{-1} are due to the attachment of additional methylene groups.[28,29] The FT-IR results indicated that a small amount of PS chains should suffice to coat on the graphene surface after melt blending. TEM observation was further applied to prove the

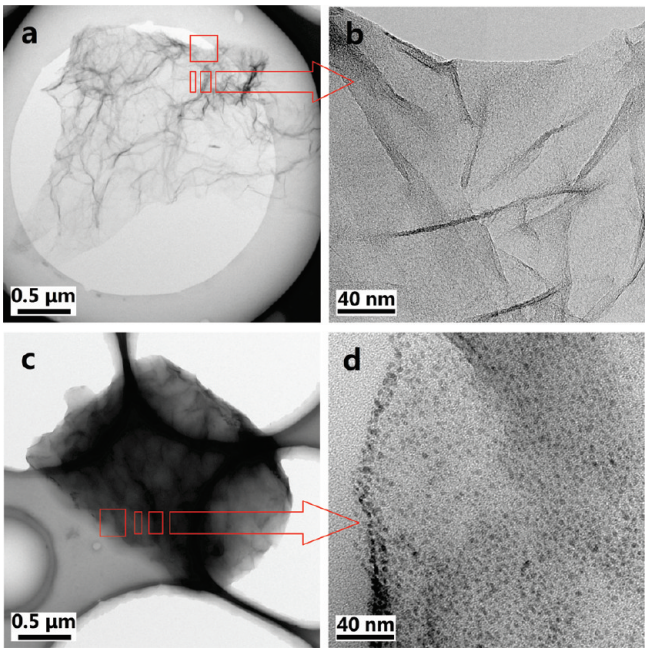

Figure 5. TEM images of (a) pristine graphene, (b) the partial enlarged view of pristine graphene, (c) PSFG60 and (d) the partial enlarged view of PSFG60.

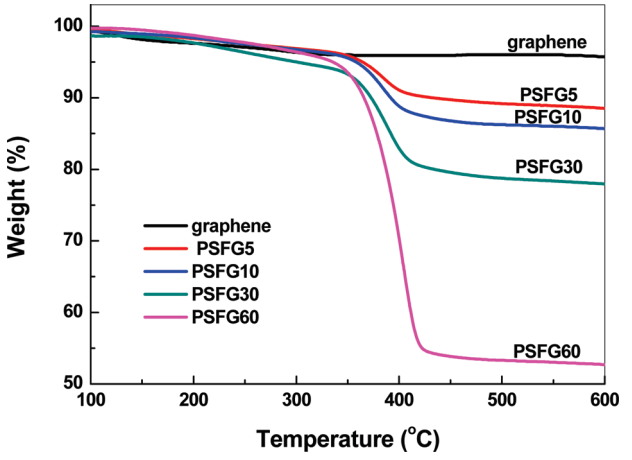

Figure 6. TGA curves of PSFG samples. Here, the PSFG were collected from the supernatants of PSG composites with various melt blending times by filtration with a 220 nm PTFE membrane and wash with toluene to remove any free PS.

formation of PSFG during the melt blending, and the results are shown in Figure 5. It is seen from Figure 5a that the pristine graphene looks like a transparent ultrathin film with a few thin ripples within the plane, which is typical for the TEM micrograph of graphene, as reported by previous research.[30] For PSFG60 sample, as shown in Figure 5c, a distinguishable layer of dark coating appears on the surface. A partial enlarged view of PSFG60 (Figure 5d) indicates that a large amount of particles with a size of 3−5 nm are coating the graphene surface. These particles were thought to belong to the PS phase because they could not be observed in the partial enlarged view of pristine graphene as shown in Figure 5b. These results demonstrate that some PS chains have been coating the surface of graphene through the interaction between graphene and PS.

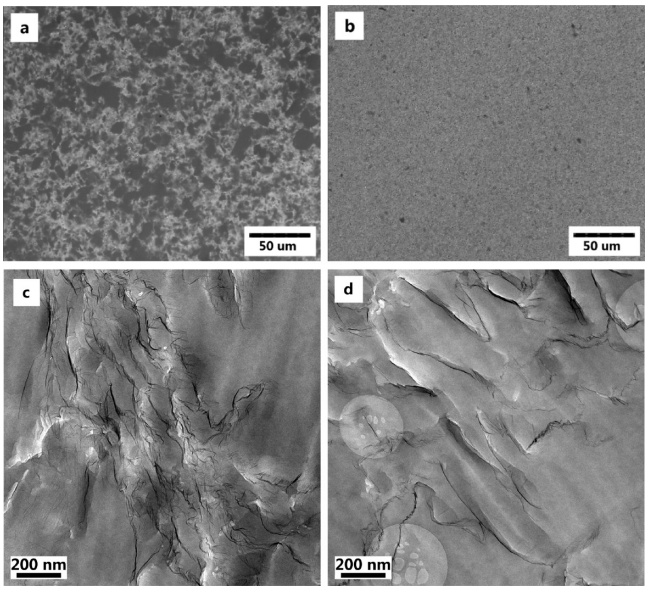

Figure 7. (a) Optical micrograph and (c) TEM image of PS/pristine graphene composite; (b) optical micrograph and (d) TEM image of PS/PSFG60 composite. The loading of graphene was about 1 wt % for each composite.

To determine the functionalized PS in PSFG samples, TGA measurements were carried out and the curves are shown in Figure 6. For the sake of comparison, the TGA data of pristine graphene was carried out as well. The weight loss of samples reached the equilibrium at a temperature of 500 °C, which was well in accord with the results described in Figure 3, indicating that all PS parts had been burned out. It is noted that the pristine graphene lost 4.0 wt % of its original weight. On the basis of these data, the functionalized PS content within PSFG samples was evaluated, and the results are shown in Table 1. For PSFG5, its PS content is 7.1 wt %. With the extension of melt blending time, the functionalized PS content increases gradually from 7.1 to 10.1 wt % for PSFG10, to 18.0 wt % for PSFG30, and to 44.5 wt % for PSFG60. The results demonstrated that the increased melt blending time facilitated the attachment of PS chains onto the surface of graphene, because of the enhanced interactions between graphene and PS components.

As an application demonstration, the PSFG dispersion was subsequently used for the preparation of PS matrix composites. For comparison, the dispersion of pristine graphene in PS matrix was also employed. Using the composites containing 1.0 wt % of pristine graphene and PSFG60 as examples, the dispersing states of pristine graphene and PSFG60 were studied in macroscopic scale by optical observation and in microscopic scale by TEM. For optical observation, each composite solution in THF was cast into a thin film with the thickness of around 10 μm. In the case of pristine graphene, many dark spots with the diameter of several micrometers are observed on the optical micrograph (Figure 7a). The TEM observation (Figure 7c) reveals that the pristine graphene particles were aggregated seriously in PS matrix. On the contrary, the composite thin film with PSFG60 seems clear and uniform (Figure 7b). Correspondingly, the TEM observation (Figure 7d) shows that the PSFG60 are uniformly distributed in the PS matrix and there are no large agglomerates observed. These results indicated the PS-functional graphene (PSFG) could disperse well in PS matrix, which may contribute

to improving some of the properties of the resultant composites, such as electric conductivity, thermal conductivity, and mechanical property.

The DC electrical conductivities of the resulting PS composites at a constant filler loading of 3.0 wt % were measured with a four-probe system (suitable for samples with conductivities higher than 1×10^{-6} S/m). As expected, PS composite with PSFG60 had a conductivity of 0.9 S/m, much higher than 0.06 S/m of the PS composite filled with pristine graphene. The higher conductivity of PS/PSFG composite was attributed to the much more homogeneous dispersion of PSFG in the PS matrix, compared with that of pristine graphene.

4. DISCUSSION

The influence of melt blending on the interactions between PS and graphene has been systematically investigated by various characterization techniques. In the following, the formation mechanism of interactions between PS and graphene are discussed.

As we know, graphene, produced by thermal exfoliation and reduction of GO, has a layered structure,[31,32] with a shape very similar to that of the silicates (e.g., montmorillonite).[33] Earlier studies[16,34−36] on nanoclay-based composites have suggested the existence of two general states of platelet dispersion in melt blending, i.e., the intercalated structure and the exfoliated structure. As similar morphologies have been observed in the literature on polymer/graphene composites, we thus suggest extension of this terminology to the PS/graphene systems. During melt blending, the graphene particles were first fractured by the extruder's shearing action. The polymer chains then diffused into the graphene interlayer because of a physical or a chemical affinity between the polymer and the graphene surface. As more polymer chains entered and went further in between the graphene sheets, the sheets appear to peel apart. Therefore, the increased melt blending time in the extruder generally improves the delamination and dispersion of graphene sheets in polymer matrix.

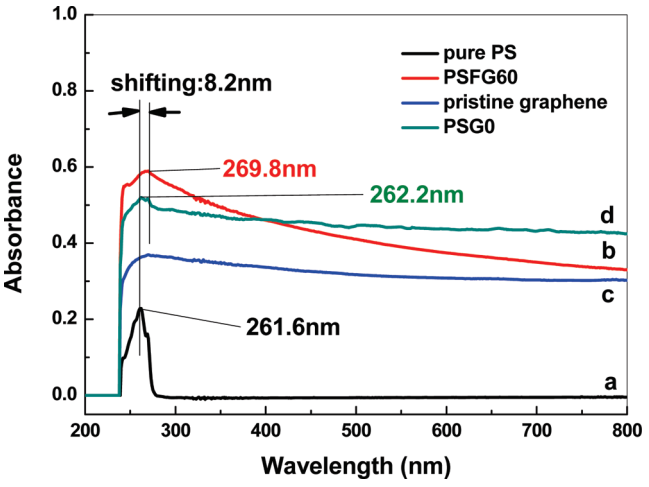

Figure 8. UV−vis absorption spectra of (a) pure PS, (b) PSFG60, (c) pristine graphene, and (d) PSG0 in $CHCl_3$.

The melt blending endowed the polymer chains with the possibility to enter the gaps of the graphene sheets. But only the formation of strong interactions between PS and graphene could stabilize the formed exfoliated structures. Generally, the aromatic structures interact strongly with the basal plane of the graphite surface through $\pi-\pi$ stacking. So certainly there may have occurred a $\pi-\pi$ stacking between the aromatic system of π-electrons of PS and the π-electrons system of the graphene in PS/graphene composite during the melt blending. A UV−vis absorption spectroscopy was carried out to confirm this supposition, and the results are shown in Figure 8. The spectrum of pristine graphene (Figure 8c) does not exhibit any meaningful peaks, whereas that of pure PS, PSG0, and PSFG60 exhibit a clear absorption peak of phenyl groups. Obviously, the peak of PSFG60 (Figure 8b) shifts to a higher field by 8.2 nm compared to that of pure PS (Figure 8a). This shift is believed to have originated from the effect of the ring currents in graphene and PS π-systems.[37] In comparison, there is essentially no obvious shift for the peak of PSG0 (Figure 8d) prepared by only solution mixing. Such shifting feature is attributed to the formation of noncovalent $\pi-\pi$ stacking between phenyl rings of PS chains and basal planes of graphene by melt blending.

According to previous research,[38] the formation of "$\pi-\pi$ stacking" is only possible with an intermolecular distance of 3−4 Å,[39] which means that the $\pi-\pi$ stacking can only occurs in systems with spatially close-lying π orbitals. The intermolecular distance of two graphene sheets is about 3.35 Å.[40] With the assistance of intercalation in melt blending, as indicated in Figure 9, the PS chains can get close to the graphene sheets, and the π orbitals between the phenyl rings and the basal planes of graphene sheets reach the specified distance (3−4 Å), which is essential for the formation of $\pi-\pi$ stacking. Furthermore, the PS

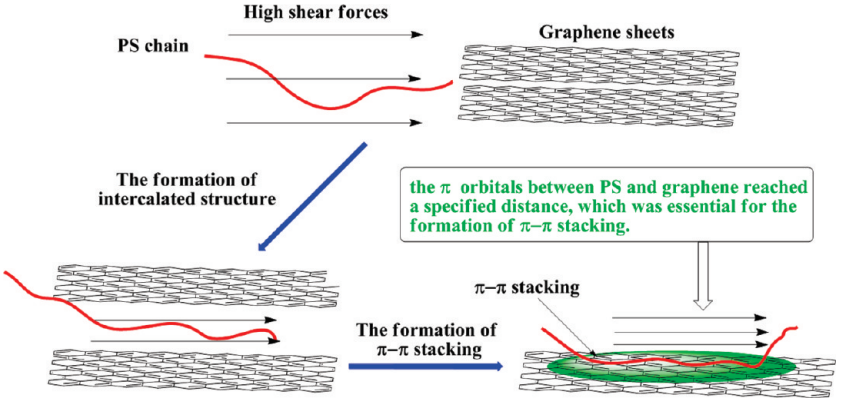

Figure 9. Schematic for the forming of $\pi-\pi$ stacking in the process of melt blending.

Table 2. Molecular Weight Changing of PS Samples with or without Melt Blending

sample name	M_n	M_w	M_w/M_n
PS without melt blending	100 300	179 600	1.79
PS with a melt blending time of 60 min	93 500	165 600	1.77

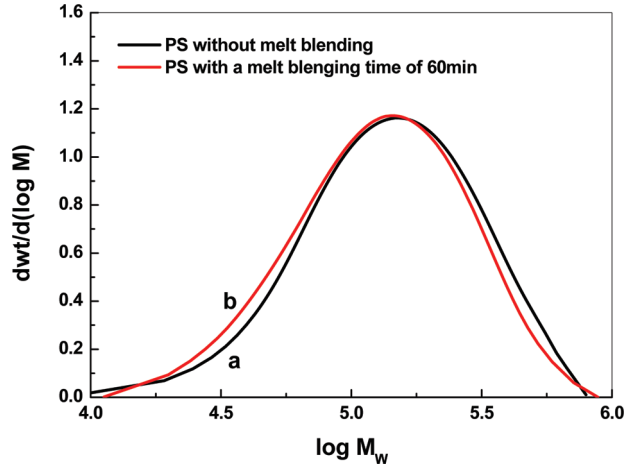

Figure 10. GPC curves of (a) PS without melt blending and (b) PS with a melt blending time of 60 min.

chains could also be stretched by the high shear forces, and a number of closely aligned aromatic rings parallel to the graphene sheet were formed, which could optimize their mutual interactions[41] and increase the overall interaction between PS and graphene. Therefore, the PS chains could be strongly adsorbed on the graphene surface through $\pi-\pi$ stacking. Moreover, the increased melt blending time in the extruder generally improves the delamination and dispersion of graphene sheets in polymer matrix. And the homogeneously dispersed graphene sheets provide maximal surface area for $\pi-\pi$ stacking with PS chains,[42] leading to more PS chains absorbed onto the graphene surface through $\pi-\pi$ stacking. However, the direct solution mixing of PS and graphene could not induce a somewhat similar $\pi-\pi$ stacking. The most probable reason is that the PS chains and the graphene sheets could not get close enough to each other to form the close-lying π orbitals, because of the strong van der Waals forces between them.

In addition to the $\pi-\pi$ stacking, the formation of chemical bonding between PS and graphene may also enhance the interaction. The effect of melt blending on the molecular weight of PS was investigated by GPC, and the results are shown in Figure 10 and Table 2. The melt blending decreased the M_n from 100 300 to 93 500, and the M_w from 179 600 to 165 600, indicating a slight degradation of PS,[43] which might have led to the formation of PS macromolecular radicals. With respect to a number of solid inorganic powders, such as graphite, carbon black, quartz, silica, TiO_2, and ZnO, it is generally recognized that, under mechanochemical mixing, a rupture of the atom-type chemical bonding takes place, and thus, many free radicals or ion-type active centers with high reactivity are created on the fresh surface.[44−46] These active sites are not only capable of initiating the polymerization of many monomers,[44,46] but also grafting already formed polymer chains, such as polyethylene, polystyrene and polypropylene.[47] In our study, during melt blending with high shear forces and high temperature, free radicals or ion-type active centers with high reactivity could certainly be created on the graphene sheets with epoxide and hydroxyl on the surface. A chemical interaction was expected to occur between the active sites of graphene and PS macromolecular radicals. Therefore, during the melt blending, it was highly possible to generate macromolecular radicals and consequently to initiate the PS grafting onto the graphene sheets. A further investigation is required to understand the possible mechanism.

5. CONCLUSIONS

PS/graphene composites were prepared by solution mixing and then melt blending with various times. Based on the above experimental results, it can be concluded that the melt blending led to enhanced interactions between PS and graphene, indicated by increased amounts of PS linked to the graphene, which dramatically increased the solubility of graphene in some solvents, such as toluene. The FT-IR measurements and the direct TEM observation verified the formation of the PS-functional graphene (PSFG) during melt blending. TGA analyses were conducted to quantitatively investigate the functionalized PS content in PSFG. It was observed that a maximum functionalized PS content of 44.5% coated on the surface of graphene sheets for PSFG60. The mechanism for the in situ formation of PSFG was addressed in this study. It was proposed that the strong shear action applied by the extruder could stretch the PS chains and allow the polymer chains to diffuse into the interlayer gap of graphene sheets. Moreover, the PS chains could get close to the graphene sheets to form the $\pi-\pi$ stacking under high shear forces. The UV−vis absorption spectroscopy of PSFG presented an obvious red shift, which suggested the presence of $\pi-\pi$ stacking between PS and graphene. Besides the $\pi-\pi$ stacking, the formation of chemical bonding was also a possible reason.

■ ASSOCIATED CONTENT

Supporting Information. Description of the preparation of graphene (PDF). This material is available free of charge via the Internet at http://pubs.acs.org.

■ AUTHOR INFORMATION

Corresponding Author

*Tel.: +86 0574 8668 5256. Fax: +86 0574 8668 5186. E-mail: wtzhai@nimte.ac.cn (W.T.Z.); wgzheng@nimte.ac.cn (W.G.Z.).

■ ACKNOWLEDGMENT

The authors are grateful to the National Natural Science Foundation of China (Grant 51003115), the Ningbo Natural Science Foundation (Grant 2011A610118), and Ningbo Key Lab of Polymer Materials (Grant 2010A22001) for their financial support of this study.

■ REFERENCES

(1) Geim, A. K.; MacDonald, A. H. *Phys. Today* **2007**, *60*, 35–41.
(2) Si, Y.; Samulski, E. T. *Nano Lett.* **2008**, *8*, 1679–1682.
(3) Blake, P.; Brimicombe, P. D.; Nair, R. R.; Booth, T. J.; Jiang, D.; Schedin, F.; Ponomarenko, L. A.; Morozov, S. V.; Gleeson, H. F.; Hill, E. W.; Geim, A. K.; Novoselov, K. S. *Nano Lett.* **2008**, *8*, 1704–1708.
(4) Li, X.; Wang, X.; Zhang, L.; Lee, S.; Dai, H. *Science* **2008**, *319*, 1229–1232.

(5) Miranda, R.; Vazquez de Parga, A. L. *Nat Nano* **2009**, *4*, 549–550.
(6) Wang, G.; Shen, X.; Wang, B.; Yao, J.; Park, J. *Carbon* **2009**, *47*, 1359–1364.
(7) Wang, G.; Yang, J.; Park, J.; Gou, X.; Wang, B.; Liu, H.; Yao, J. *J. Phys. Chem. C* **2008**, *112*, 8192–8195.
(8) Stankovich, S.; Dikin, D. A.; Piner, R. D.; Kohlhaas, K. A.; Kleinhammes, A.; Jia, Y.; Wu, Y.; Nguyen, S. T.; Ruoff, R. S. *Carbon* **2007**, *45*, 1558–1565.
(9) Geng, Y.; Wang, S. J.; Kim, J.-K. *J. Colloid Interface Sci.* **2009**, *336*, 592–598.
(10) Kuilla, T.; Bhadra, S.; Yao, D.; Kim, N. H.; Bose, S.; Lee, J. H. *Prog. Polym. Sci.* **2010**, *35*, 1350–1375.
(11) Hu, H.; Wang, X.; Wang, J.; Wan, L.; Liu, F.; Zheng, H.; Chen, R.; Xu, C. *Chem. Phys. Lett.* **2010**, *484*, 247–253.
(12) Zhao, Y. F.; Xiao, M.; Wang, S. J.; Ge, X. C.; Meng, Y. Z. *Compos. Sci. Technol.* **2007**, *67*, 2528–2534.
(13) Eda, G.; Chhowalla, M. *Nano Lett.* **2009**, *9*, 814–818.
(14) Stankovich, S.; Dikin, D. A.; Dommett, G. H. B.; Kohlhaas, K. M.; Zimney, E. J.; Stach, E. A.; Piner, R. D.; Nguyen, S. T.; Ruoff, R. S. *Nature* **2006**, *442*, 282–286.
(15) Cheah, K.; Simon, G. P.; Forsyth, M. *Polym. Int.* **2001**, *50*, 27–36.
(16) Ginzburg, V. V.; Gendelman, O. V.; Manevitch, L. I. *Phys. Rev. Lett.* **2001**, *86*, 5073.
(17) Ding, W.; Eitan, A.; Fisher, F. T.; Chen, X.; Dikin, D. A.; Andrews, R.; Brinson, L. C.; Schadler, L. S.; Ruoff, R. S. *Nano Lett.* **2003**, *3*, 1593–1597.
(18) Zhang, Z.; Zhang, J.; Chen, P.; Zhang, B.; He, J.; Hu, G.-H. *Carbon* **2006**, *44*, 692–698.
(19) Kalaitzidou, K.; Fukushima, H.; Drzal, L. T. *Compos. Sci. Technol.* **2007**, *67*, 2045–2051.
(20) Kalaitzidou, K.; Fukushima, H.; Drzal, L. T. *Composites, Part A* **2007**, *38*, 1675–1682.
(21) Kalaitzidou, K.; Fukushima, H.; Drzal, L. T. *Carbon* **2007**, *45*, 1446–1452.
(22) Kim, S.; Do, I.; Drzal, L. T. *Polym. Compos.* **2010**, *31*, 755–761.
(23) Uhl, F. M.; Yao, Q.; Nakajima, H.; Manias, E.; Wilkie, C. A. *Polym. Degrad. Stab.* **2005**, *89*, 70–84.
(24) Chen, D.; Wang, X.; Liu, T.; Wang, X.; Li, J. *ACS Appl. Mater. Interfaces* **2010**, *2*, 2005.
(25) Chen, D.; Zhu, H.; Liu, T. *ACS Appl. Mater. Interfaces* **2010**, *2*, 3702.
(26) Zhang, H.-B.; Yan, Q.; Zheng, W. G.; He, Z.; Yu, Z. Z. *ACS Appl. Mater. Interfaces* **2011**, *3*, 918–924.
(27) Peigney, A.; Laurent, C.; Flahaut, E.; Bacsa, R. R.; Rousset, A. *Carbon* **2001**, *39*, 507–514.
(28) Chen, G.; Liu, S.; Chen, S.; Qi, Z. *Macromol. Chem. Phys.* **2001**, *202*, 1189–1193.
(29) Liang, C. Y.; Krimm, S. *J. Polym. Sci.* **1958**, *27*, 241–254.
(30) Zhang, H.-B.; Zheng, W. G.; Yan, Q.; Yang, Y.; Wang, J. W.; Lu, Z. H.; Ji, G. Y.; Yu, Z. Z. *Polymer* **2010**, *51*, 1191–1196.
(31) McAllister, M. J.; Li, J. L.; Adamson, D. H.; Schniepp, H. C.; Abdala, A. A.; Liu, J.; Herrera-Alonso, M.; Milius, D. L.; Car, R.; Prud'homme, R. K.; Aksay, I. A. *Chem. Mater.* **2007**, *19*, 4396–4404.
(32) Schniepp, H. C.; Li, J.-L.; McAllister, M. J.; Sai, H.; Herrera-Alonso, M.; Adamson, D. H.; Prud'homme, R. K.; Car, R.; Saville, D. A.; Aksay, I. A. *J. Phys. Chem. B* **2006**, *110*, 8535–8539.
(33) Paul, D. R.; Robeson, L. M. *Polymer* **2008**, *49*, 3187–3204.
(34) Zhao, J.; Morgan, A. B.; Harris, J. D. *Polymer* **2005**, *46*, 8641–8660.
(35) Dennis, H. R.; Hunter, D. L.; Chang, D.; Kim, S.; White, J. L.; Cho, J. W.; Paul, D. R. *Polymer* **2001**, *42*, 9513–9522.
(36) Potts, J. R.; Dreyer, D. R.; Bielawski, C. W.; Ruoff, R. S. *Polymer* **2011**, *52*, 5–25.
(37) Allcock, H. R. *Adv. Mater.* **1994**, *6*, 106–115.
(38) Grimme, S. *Angew. Chem., Int. Ed.* **2008**, *47*, 3430–3434.
(39) Hunter, C. A.; Sanders, J. K. M. *J. Am. Chem. Soc.* **1990**, *112*, 5525–5534.
(40) de Andres, P. L.; Ram; iacute; rez, R.; Verg; eacute; s, J. A. *Phys. Rev. B* **2008**, *77*, 045403.
(41) Yang, M.; Koutsos, V.; Zaiser, M. *J. Phys. Chem. B* **2005**, *109*, 10009–10014.
(42) Wu, H.; Zhao, W.; Hu, H.; Chen, G. *J. Mater. Chem.* **2011**, *21*, 8626–8632.
(43) Pospísil, J.; Horák, Z.; Krulis, Z.; Nespurek, S.; Kuroda, S.-i. *Polym. Degrad. Stab.* **1999**, *65*, 405–414.
(44) Kargin, V. A.; Platé, N. A. *J. Polym. Sci.* **1961**, *52*, 155–158.
(45) Hasegawa, M.; Ogata, T.; Sato, M. *Powder Technol.* **1995**, *85*, 269–274.
(46) Hasegawa, M.; Kimata, M.; Kobayashi, S.-I. *J. Appl. Polym. Sci.* **2001**, *82*, 2849–2855.
(47) Ruan, W. H.; Zhang, M. Q.; Rong, M. Z.; Friedrich, K. *Polym. Polym. Compos.* **2004**, *12*, 257–267.